Macromolecules
ARTICLE

Macromolecules **2009**, *42*, 7913–7918 **7913**
DOI: 10.1021/ma901347r

Role of Surface Reorganization on Preferential Adsorption of Macromolecular Ensembles at the Solid/Fluid Interface

Juan Pablo Hinestrosa,[†] Jose Alonzo,[†] Jimmy W. Mays,[‡,§] and S. Michael Kilbey II*[,‡,§]

[†]*Department of Chemical and Biomolecular Engineering, Clemson University, Clemson, South Carolina 29634,* [‡]*Department of Chemistry, University of Tennessee, Knoxville, Tennessee 37996, and* [§]*Center for Nanophase Materials Sciences, Oak Ridge National Laboratory, Oak Ridge, Tennessee 37831*

Received June 23, 2009; Revised Manuscript Received September 3, 2009

ABSTRACT: The adsorption of micelles made from precisely synthesized branched block copolymers is investigated and analyzed using a model framework that incorporates the effects of mass transport and dynamic relaxation/reorganization events occurring at the solid/fluid interface. Both processes are required to represent adequately the adsorption profile over the entire progression to pseudoequilibrium. Insight into the relative importance of the two processes, the terminus of the diffusion-dominated regime, and differences between diffusion in free solution and in confinement is also provided. The results demonstrate commonality between adsorption of micelle-forming surfactant-like copolymers and biomimetic vesicles formed by small-molecule surfactants, both of which are systems dominated by rearrangements on the surface.

Introduction

The adsorption of complex soft matter at interfaces is relevant to a variety of chemical and biological phenomena and central to the promise of preferential adsorption as a scalable and robust method of materials processing. Self-assembly has been proposed as an enabling technology that is suitable for the fabrication of a variety of next-generation devices and systems, such as nanopatterned resists for advanced lithography electronic circuitry and biomimetic constructs.[1] In this pursuit, block copolymers having incompatible blocks are often used because rigorous and controlled synthetic strategies can be employed to tailor how chemical information is encoded into the molecule by tuning composition, connectivity, and chemical constituents.[2] In a selective solvent, block copolymers spontaneously self-assemble into complex microphase segregated ensembles.

In this article, we investigate the kinetics of preferential adsorption of self-assembled macromolecular ensembles onto solid substrates and the kinetic processes leading to the formation of tethered polymer layers, which in contrast with the thermodynamic behaviors of micellar systems in solution[1−6] is dealt with in a largely phenomenological manner. It is generally agreed that when micellar systems self-assemble at the solid/fluid interface, there is a dynamic relaxation/reorganization of the micelles that ultimately leads to the tethering of individual chains and micellar structures.[5,7−13] Rearrangement processes that may occur include breakup of the entire micelle, releasing single chains that will preferentially adsorb, or adsorption of micellar coronal arms that then lead to a redistribution of the core blocks to populate the surface and relieve the local crowding.[8] It is also speculated that in situations where there is a high energy barrier between the coronal arms and the substrate, the micelles never adsorb but act only as reservoirs, supplying free chains to the solution that may eventually tether, driving the layer formation process.[5]

Despite the agreement on the complexity of the phenomena and possible mechanisms at play during adsorption, these dynamic events are basically omitted from any mathematical description of the adsorption process. Oftentimes, the classical diffusion-controlled model, $\Gamma(t) = 2C_o(Dt/\pi)^{1/2}$, derived from Fick's second law, which depends on the initial adsorbate concentration, C_o, and the diffusion coefficient, D, is assumed to apply and is used to describe how the adsorbed amount, Γ, changes with time, t, in the early stages.[14,15] However, almost no attention is placed on identifying the true terminus of the diffusion-limited regime, verifying the $t^{1/2}$ time dependence, or properly describing adsorption behaviors at the intermediate or long times of the adsorption process. Moreover, assumptions of no interactions between approaching and adsorbed chains and that every polymer chain that reaches the surface is adsorbed immediately are dramatic simplifications and particularly problematic for large adsorbing molecules and macromolecular aggregates that have numerous conformational states and are in dynamic equilibrium with single chains. As a result, values of D extracted by fitting the experimental data in early stages of the self-assembly process often deviate substantially, sometimes by several orders of magnitude, from values typically expected.[1,3,7−11,16−18] While successful for describing the adsorption of single polymer chains[14,15] and the sequential adsorption of homopolymers,[19] the Fickian diffusion-controlled model has proven to be unsuccessful for linear diblock copolymers forming polymer brushes[16] and more complex systems such as high-molecular-weight triblock copolymers[17] and polyelectrolyte micelles.[11] To examine the importance of dynamic relaxation/reorganization processes occurring at the solid/fluid interface, preferential adsorption of polymer micelles onto Si/SiO_2 surfaces is monitored in situ by phase-modulated ellipsometry, allowing their adsorption kinetics to be studied in real time.

Experimental Section

Materials and Sample Preparation. Miktoarm PS−PI−$(PI)_2$ branched block copolymers were synthesized via anionic polymerization using chlorosilane coupling to graft two PI anions and a PS−PI diblock copolymer at a junction. (See Figure 1a.) This scheme exploits methods pioneered by Mays and Hadjichristidis,

*Corresponding author. E-mail: kilbeysmii@ornl.gov.

Published on Web 09/25/2009

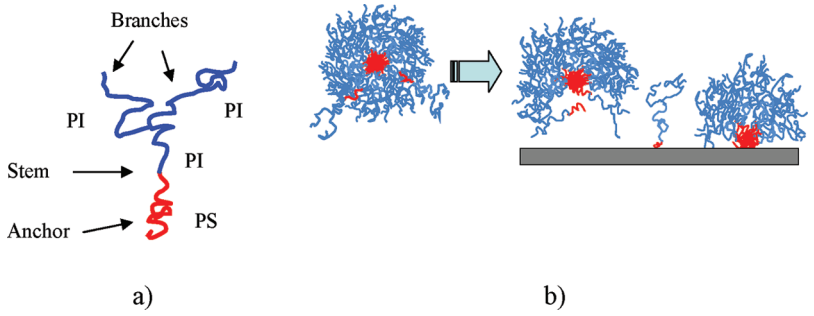

Figure 1. (a) Illustration of a single PS−PI−$(PI)_2$ miktoarm copolymer. (b) Cartoon depicting the preferential adsorption of macromolecular ensembles onto silicon substrates from *n*-hexane solutions.

Table 1. Properties of Polystyrene−Polyisoprene (PS−PI) Diblock and PS−PI−$(PI)_2$ Miktoarm Copolymers, With Block Molecular Weights Given in kilodaltons

sample ID and block M_w		M_w PS (kDa)	M_w PI (kDa)	PDI	dn/dc	D_s (cm^2/s)[b]	R_g/R_h[b]
DB[a]	PS−PI 26/141	26	141	1.09	0.224	8.7×10^{-8}	0.78
MA1	PS−PI−$(PI)_2$ 33/33/$(14)_2$	33	60	1.01	0.219	1.7×10^{-7}	0.62
MA3	PS−PI−$(PI)_2$ 29.6/70/$(43)_2$	29.6	156	1.17	0.207	1.2×10^{-7}	0.73
MA4	PS−PI−$(PI)_2$ 33/33/$(57.8)_2$	33	149	1.14	0.199	1.1×10^{-7}	0.73

[a] Obtained from Polymer Source, Inc. [b] Results obtained from static and dynamic light scattering at $C_o = 30\ \mu$g/mL in *n*-hexane.

whereby living macroanions are coupled using chlorosilanes to afford branched architectures, as recently reviewed.[20] Here a poly(styrene-*block*-isoprenyl)-lithium anion is reacted with a considerable excess of trichlorosilane. After recovery of the dichlorosilane end-capped PS-PI diblock, the separately made poly(isoprenyl)-lithium "arms" are introduced and allowed to react to give the miktoarm product. This method not only allows the constituents to be characterized, but styrene and isoprene monomers are among the best behaved monomers for living anionic polymerization, producing well-defined structures that promote fundamental studies of effects such as polymer architecture, block size, composition, and solvent quality. Also, a PS-PI diblock copolymer and a PI homopolymer were obtained from Polymer Source (Montreal, Canada) to allow useful comparisons because the molecular weights (M_w) of their blocks are very similar to those of the miktoarm copolymers. Table 1 shows the properties of all copolymers used, with the molecular weights of each block of the PS−PI−PI_2 copolymers given in kilodaltons following the sample identification string.

Stock solutions having a concentration of 300 μg/mL were prepared by the addition of 60 mL of *n*-hexane (99%, Alfa Aesar) to 18 mg of bulk polymer. The *n*-hexane was filtered through Millpore 0.2 μm PTFE filters prior to solution preparation. The stock solutions were sealed and gently shaken for at least 10 days at room temperature to allow for equilibration. Prior to an experiment (48−72 h), an aliquot was taken from the stock solution and diluted with filtered *n*-hexane to achieve the desired experimental concentration at which the kinetics experiments were performed. Concentrations of 30 and 3 μg/mL were employed for the adsorption studies.

We cleaned diced silicon wafers (1.2 cm × 1 cm) obtained from Silicon Quest by immersing them in "piranha acid", a 70/30 (v/v) sulfuric acid (98%)/hydrogen peroxide (30%) mixture, at 110 °C for 30 min. *Piranha acid is a strong oxidizer; contact with organic solvents must be avoided, and the solution should not be left unattended.* After the wafers were extracted from the piranha acid bath, they were rinsed with copious amounts of distilled water and dried with filtered N_2. This cleaning process leaves a silicon oxide, SiO_x, layer of thickness between 13 and 15 Å, as checked by ellipsometry. These wafers were used within 4 h of preparation. The glass fluid cell used to conduct the kinetics experiments was also cleaned in piranha acid in the same manner as the silicon wafers, except it was also rinsed with filtered acetone (0.2 μm PTFE Millpore) before the N_2 drying.

Phase-Modulated Ellipsometry. The kinetics of self-assembly at the solid/liquid interface is monitored using a Beaglehole Picometer Ellipsometer, which uses a He−Ne laser light source ($\lambda = 632.8$ nm) and a photoelastic birefringent (quartz) element to modulate the phase of the incident light beam. Phase modulation provides a higher sensitivity, lower signal-to-noise ratio, and a time resolution as short as 1 s. The design of the phase modulation element includes a gauge crystal for feedback monitoring, and thus slight variations in the system do not affect the experiments. Ellipsometry is a technique that measures the real and imaginary components of the ellipsometric ratio, ρ, which is defined as[16]

$$\rho = \frac{r_p}{r_s} = \tan \Psi e^{i\Delta} = \mathrm{Re}(\rho) + i\mathrm{Im}(\rho) \qquad (1)$$

where $\mathrm{Re}(\rho) = \tan\Psi \cos\Delta$ and $\mathrm{Im}(\rho) = \tan\Psi \sin\Delta$ and r_p and r_s are the complex overall reflection coefficients of the *p* and *s* polarization states, respectively. The angle Ψ corresponds to the ratio of attenuation of the *p*- and *s*-polarizations, and the angle Δ corresponds to the respective phase shift.

At the start of the experiment, a clean silicon wafer is mounted on a home-built stage that fits in a cylindrical fluid cell made of high-quality optical glass. The entire fluid cell assembly sits on an *x*-, *y*-, *z*-translation stage that can also be tilted (rotated) about principle axes coincident with and perpendicular to the plane formed by the *p* and *s* polarization states of the incident light beam. This allows the sample to be aligned such that the laser beam goes in (and exits) normal to the walls of the fluid cell, impinges on the center of the wafer, and cleanly enters the detector through a pinhole. The alignment procedure is performed at incident angles of 75 and 40°. Then, the fluid cell is filled with ~13 mL of filtered (Millpore PTFE 0.2 μm) *n*-hexane and, if necessary, realigned so the laser beam again passes cleanly through the pinhole at 75 and 40°. After the system is aligned, the arms that hold the incident and detector optics and electronics are moved in tandem to the Brewster angle, defined by $\theta_B = \tan^{-1}(n_{substrate}/n_{solvent})$, where $n_{substrate}$ is the refractive index of silicon (3.875) and $n_{solvent}$ is the refractive index of *n*-hexane (1.372); therefore, for this system, $\theta_B \approx 70.5°$, and under this condition, $\Delta = 90$ and $\mathrm{Re}(\rho) = 0$. Experimentally, the Brewster angle is determined by finding the angle at which $\mathrm{Re}(\rho) < 1 \times 10^{-3}$, nominally $\theta_B = 70.5 \pm 0.3°$. After θ_B is determined, the imaginary signal, $\mathrm{Im}(\rho)$, is followed for about 1000 s to establish a baseline and determine if any contamination has adsorbed on the surface. Imaginary baseline signal

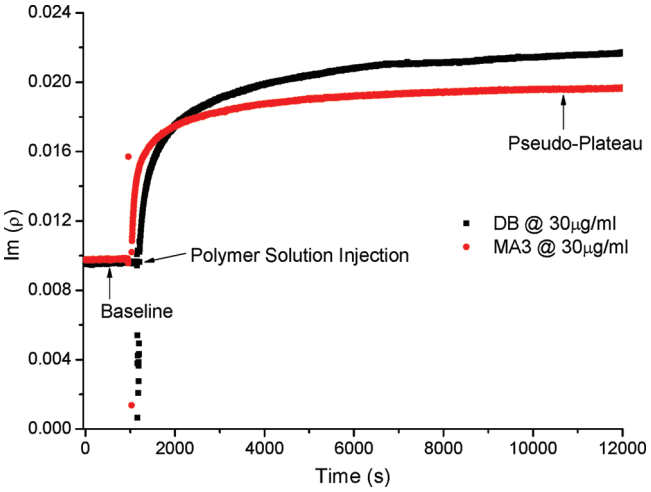

Figure 2. Measured Im(ρ) signal for the adsorption of PS-PI 26/141 (DB) and PS−PI−$(PI)_2$ 29.6/70/$(43)_2$ (MA3) onto silicon substrates from *n*-hexane solutions.

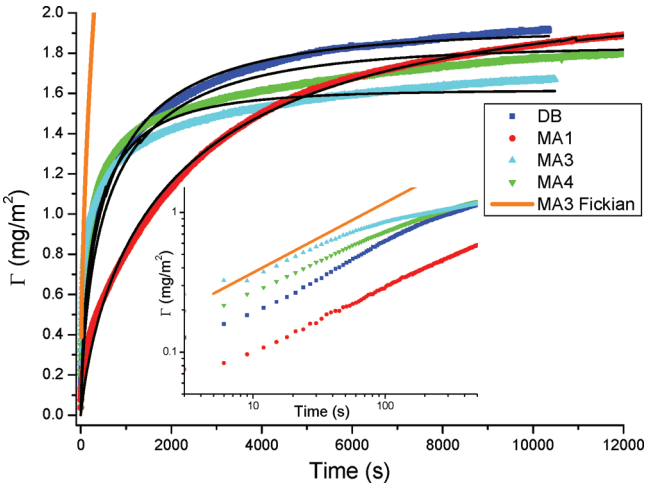

Figure 3. Profiles showing kinetics of adsorption of PS−PI−$(PI)_2$ micelles formed in *n*-hexane onto silicon substrates. The solid colored lines are the experimental data, and the black lines are the fitting results obtained using eq 3. The solid orange line corresponds to an adsorption profile calculated using the Fickian diffusion-limited model, $\Gamma(t) = 2C_o(D_s t/\pi)^{1/2}$. The inset presents a log−log plot of the adsorption profiles up to 500 s.

values of Im(ρ) = 9.6×10^{-3} are typically obtained for silicon in *n*-hexane, with deviations of the repeated measurements being $\pm 3.9 \times 10^{-5}$, or roughly 5 parts in 1000. This demonstrates the accuracy of the measurement and suitability of the phase-modulated ellipsometer to resolve very small changes in surface conditions. If the baseline remains stable, then the solvent is drained from the cell and replaced with a polymer solution (filtered through a Millpore PTFE 0.2 μm filter) at the desired concentration, and the measurement is quickly started. The Im(ρ) signal is recorded every 3 s until a pseudoplateau in its signal is reached. An illustration of the micellar adsorption process is shown in Figure 1b, and data showing the evolution of the imaginary signal from the baseline to the pseudoequilibrium are shown in Figure 2. The reported results are the average of at least three repeated experiments, and we have found <7% variation between them. The adsorbed amount, Γ (in milligrams per meters squared), which is the areal density of polymer adsorbed on the substrate, is calculated from Im(ρ) using the following equation[16]

$$\mathrm{Im}(\rho) - \mathrm{Im}(\rho)_{\mathrm{baseline}} = \frac{2\pi}{\lambda} \frac{\sqrt{n_{\mathrm{solvent}}^2 + n_{\mathrm{substrate}}^2}}{n_{\mathrm{solvent}}} \left(\frac{\mathrm{d}n}{\mathrm{d}c}\right) \Gamma \qquad (2)$$

Here λ is the laser beam wavelength, and the refractive index increment, dn/dc, values are determined independently at 25 °C for each sample using a Wyatt Technology Optilab rEX refractive index detector (λ = 658 nm) in conjunction with a Harvard Apparatus PHD 2000 infusion syringe pump. The experimentally determined dn/dc values are reported in Table 1.

Results and Discussion

Figure 3 shows the adsorption profiles for the miktoarm copolymers at C_o = 30 μg/mL with an inset log−log plot showing the first 500 s of the adsorption process. For comparison purposes, the kinetics of adsorption predicted for MA3 based on a Fickian diffusion-limited model using the experimentally measured[21] diffusion coefficient in solution, D_s, is also shown. The adsorption at early times, <100 s, is very fast because of the large number of available sites, the diffusion of the macromolecular ensembles, and the rapid introduction of the polymer solution into the fluid cell. Following this initial period, there is a transition marked by continuously slowing the adsorption rate until a pseudoplateau is reached at ~12 000 s. At these long times, the layer is considered to be fully formed as repulsion between the copolymers chains of the adsorbed layer shields the surface, creating a significant barrier to penetration and tethering of additional chains or supramolecular ensembles. As seen in the inset of Figure 3, the adsorption profile calculated using a Fickian diffusion-limited model for sample MA3 shows substantial and increasing deviation from the data after the first 30 s, suggesting both the end of the diffusion-limited regime and the limit of applicability of the Fickian model.

Control experiments using a PI hompolymer showed negligible adsorption (Γ = 0.14 mg/m^2 at 10 000 s) at the highest concentration studied. (See the Supporting Information.) Static and dynamic light scattering (SLS and DLS) were carried out to determine the self-diffusion coefficient in solution, D_s, hydrodynamic radii, R_h, and radius of gyration, R_g, in the selective solvent *n*-hexane. This work will be described in a subsequent article.[21] As seen from the values shown in Table 1, the ratios $R_g/R_h \approx 0.7$ suggest that the branched PS−PI−$(PI)_2$ copolymers form spherical "hairy" micelles in *n*-hexane, having corona made of the PI−$(PI)_2$ blocks and a solvophobic PS core.[21] These findings, along with a larger spreading coefficient, S, for PS in comparison with PI,[22] suggest that there is an initial interaction of the coronal blocks with the substrate and a subsequent reorganization of the ensembles to expose the insoluble PS core blocks to generate the polymer layer. (See the Supporting Information for calculations of S.) It is interesting to note that the adsorption behavior of sample MA1, which has the shortest PI−$(PI)_2$ block ($M_{w,PI}$ = 60 kDa) and smallest M_w and R_h, exhibits an extended transition period in its approach to pseudoequilibrium and achieves the largest Γ at long times (12 000 s). The transition toward the pseudoequilibrium occurs at shorter times for the branched samples MA3 and MA4 ($t \approx 700$ s) in comparison with the linear sample DB ($t \approx 1000$ s). This behavior is due to the increased difficulty for chain penetration and adsorption posed by the branched adsorbed macromolecules compared to linear adsorbed chains.

Given that the diffusion-limited regime ends within a few seconds and because there is negligible homopolymer adsorption, we now test the suitability of the model proposed by Hubbard and coworkers,[23] which was conceived to describe the formation of hybrid bilayer membranes by adsorption, rupture, and surface fusion of vesicles, as a framework for characterizing the dynamic processes by which complex macromolecular surfactant-like systems self-assemble at the solid-fluid interface. To the best of our knowledge, this model has been used only by the original

Table 2. Adsorption Kinetics Fitting Results

sample ID	C_o (μg/mL)	K (cm/s)	D_{eff} (cm^2/s)	Γ_m (mg/m^2)	K^2/D_{eff} (s^{-1})
DB	30	$6.00 \times 10^{-5} \pm 1.05 \times 10^{-9}$	$5.67 \times 10^{-8} \pm 2.13 \times 10^{-9}$	$1.92 \pm 1.0 \times 10^{-3}$	6.35×10^{-2}
MA1	30	$8.76 \times 10^{-5} \pm 9.16 \times 10^{-9}$	$2.39 \times 10^{-8} \pm 3.09 \times 10^{-11}$	$2.08 \pm 0.7 \times 10^{-3}$	3.21×10^{-1}
MA3	30	$7.00 \times 10^{-5} \pm 2.17 \times 10^{-9}$	$7.91 \times 10^{-8} \pm 6.86 \times 10^{-10}$	$1.62 \pm 1.3 \times 10^{-3}$	6.19×10^{-2}
MA4	30	$4.00 \times 10^{-5} \pm 2.63 \times 10^{-9}$	$5.54 \times 10^{-8} \pm 3.29 \times 10^{-10}$	$1.84 \pm 8.7 \times 10^{-3}$	2.88×10^{-2}
MA1[a]	3	$3.56 \times 10^{-6} \pm 4.03 \times 10^{-9}$		$1.51 \pm 1.0 \times 10^{-3}$	
MA3	3	$1.29 \times 10^{-5} \pm 1.06 \times 10^{-8}$	$1.42 \times 10^{-7} \pm 1.46 \times 10^{-10}$	$1.07 \pm 4.4 \times 10^{-3}$	1.17×10^{-3}
MA4	3	$8.00 \times 10^{-5} \pm 4.86 \times 10^{-8}$	$5.51 \times 10^{-7} \pm 2.94 \times 10^{-10}$	$1.49 \pm 1.5 \times 10^{-3}$	1.16×10^{-2}

[a] Fitting results using eq 5 were better than those obtained using eq 3.

authors to explain the formation of biomimetic cell membranes[23] and tested in limiting cases by Tirrell and coworkers[24] to describe the kinetics of bilayer formation by vesicle adsorption on silicon substrates. The model allows the evolution of Γ to be followed as a function of t with the adsorption rate depending on the fraction of surface sites available[23]

$$\Gamma(t) = \Gamma_m \left\{ 1 - \exp\left[\frac{-KC_o}{\Gamma_m} \left[\frac{D_{eff}}{K^2} \left(\exp\left[\frac{K^2 t}{D_{eff}} \right] \operatorname{erfc}\left[\left(\frac{K^2 t}{D_{eff}} \right)^{1/2} \right] - 1 \right) + \frac{2}{K} \left(\frac{D_{eff} t}{\pi} \right)^{1/2} \right] \right] \right\} \quad (3)$$

Here Γ_m is the maximum adsorbed amount, D_{eff}, is a near-surface (effective) diffusion coefficient, and K is the surface reorganization parameter that accounts for the variety of dynamic relaxation/reorganization processes previously described that may occur at the interface during adsorption. Equation 3 is derived on the basis of an imperfectly adsorbing substrate having a near-surface concentration gradient and also satisfies the initial condition $\Gamma_{(t=0)} = 0$ and boundary condition $\Gamma_{(t=\infty)} = \Gamma_m$.[23] The parameter K^2/D_{eff} represents the relative contribution of mass transport to surface relaxation/reorganization effects. Larger values of K^2/D_{eff} correspond to a mass transport limited regime, whereas smaller values of K^2/D_{eff} imply that layer formation is governed by complex surface relaxation/reorganization events. On the basis of this, two limiting cases are predicted. For larger values of K^2/D_{eff}, surface reorganization processes are fast and the adsorption is diffusion limited[23]

$$\Gamma(t) = \Gamma_m \left[1 - \exp\left(\frac{-2C_o}{\Gamma_m} \left(\frac{D_{eff} t}{\pi} \right)^{1/2} \right) \right] \quad (4)$$

When the evolution of the layer is limited by surface relaxation/reorganization events, the adsorption process is modeled by[23]

$$\Gamma(t) = \Gamma_m \left[1 - \exp\left(\frac{-KC_o t}{\Gamma_m} \right) \right] \quad (5)$$

To characterize the adsorption of the branched block copolymer micelles, eq 3 was used to fit the adsorption profiles using the Marquardt−Levenberg algorithm with K, D_{eff}, and Γ_m as fitting parameters. The model is parametrized using D_s as the initial value for D_{eff} and with Γ_m set equal to the Γ measured from the pseudoplateau at ~12 000 s. The parameter C_o is known and not allowed to vary. Finally, an initial value of $K = 1 \times 10^{-5}$ cm/s is used, which is similar to what was previously obtained by Hubbard et al.[23] and Strompoulis et al.[24] to describe vesicle adsorption. Values of K, D_{eff}, and Γ_m obtained by fitting the adsorption profiles at $C_o = 30$ and 3 μg/mL are shown in Table 2. All parameters obtained from the fits show low correlation coefficients (0.2 to 0.5), providing evidence that eq 3 is not overspecified and that D_{eff}, K, and Γ_m are needed to characterize the self-assembly of these macromolecular aggregates at the solid/fluid interface effectively.

It is clear from Figure 3 and Table 2 that the "mixed-controlled" model embodied by eq 3 accurately predicts the entire adsorption kinetics profiles. The predicted Γ_m values are slightly lower than (within 10% of) the experimentally measured values, and the adsorption behavior at early times has been adequately captured. In agreement with experimental results, the model also predicts that adsorption of MA1 yields the largest Γ_m, which is consistent with the idea that its smaller micelle size allows more micelles to pack along the solid/fluid interface. This result is in agreement with the work of Bijsterbosch et al.,[25] who studied the effect of micelle size on adsorption using micelles made from poly(dimethyl siloxane)-*block*-poly(2-ethyl-2-oxazoline) copolymers in aqueous solution. While in their system, the adsorption kinetics are governed by an interchange between the micelles and the free chains in solution; they found that at constant concentration, as the size of each block is reduced, Γ increases. Because of the glassy nature of the PS blocks, it is often speculated that an exchange between micelles and free chains during the adsorption might not occur; however, it has been shown that in PS−PI micellar aggregates in *n*-heptane, the PS core is slightly solvated.[4,26] Additionally, Pispas and coworkers[27] showed that for PS−(PI)$_3$ miktoarm copolymers self-assembled in *n*-decane there is a coexistence of both micelles and unimers in solution at low concentrations.

The constituent polymers of the micelles formed from DB, MA3, and MA4 have a similar M_w and PDI, and their micellar aggregates show comparable trajectories in their adsorption behavior, with the surface layers made from the branched macromolecules having lower Γ_m and K^2/D_{eff}. We point to this as supporting the idea that differences in micellar aggregate structure (e.g., size, aggregation number, core, and coronal solvation) affect both mass transport and dynamics of surface relaxations/reorganizations, which in concert give rise to layer evolution. It is interesting to note that the linear analog of the miktoarm copolymers reaches a pseudoequilibrium Γ value only slightly less than that of the smallest miktoarm (MA1). One of the relaxation/reorganization processes that might occur during the adsorption process is the release of single chains, and it has been shown that the passage of the chain through the corona is the rate-determining step in this type of relaxation.[28] Therefore, it is reasonable to assume that it would be easier for a linear chain embedded in micelle to extract itself from the ensemble and find an adsorption site on the substrate, thus influencing the kinetic process. In terms of the preferential adsorption behavior of the miktoarm samples, from Table 2 it is observed that MA1 has the largest K^2/D_{eff} value in comparison with MA3 and MA4. This is

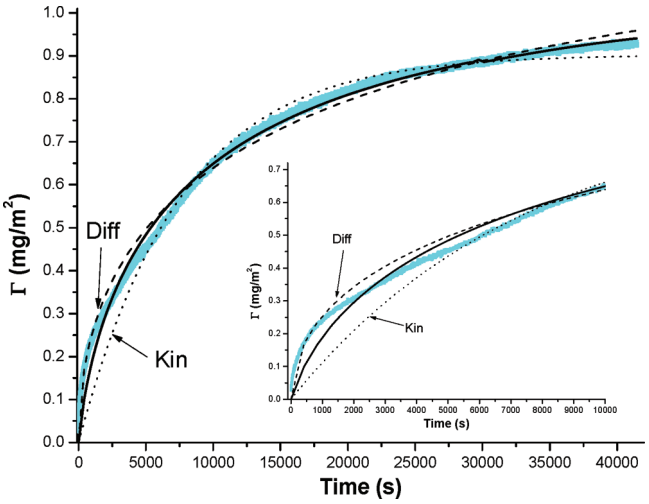

Figure 4. Adsorption of MA3 at C_o = 3 μg/mL from *n*-hexane onto silicon substrates. The light blue solid line is the experimental data. The solid black line is the fitting result using eq 3, whereas the dashed line is the fit obtained using eq 4 and the dotted line is the fitting results based on eq 5. The inset shows the same profile and fits up to t = 10 000 s.

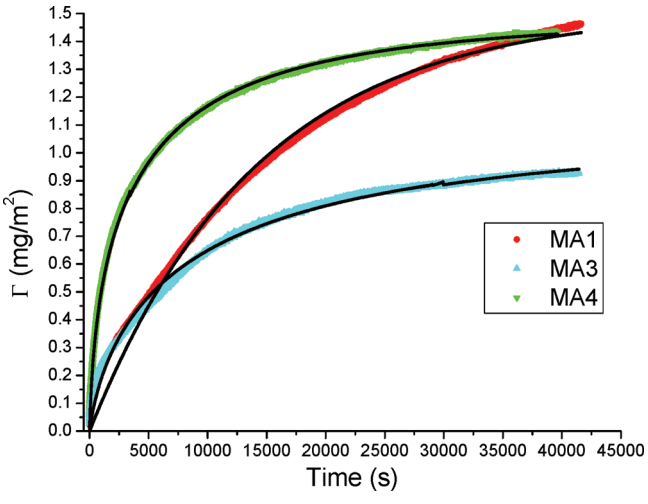

Figure 5. Adsorption profiles of PS−(PI)−$(PI)_2$ miktoarm copolymers onto silicon substrates from *n*-hexane at C_o = 3 μg/mL. The black solid lines are the best-fits obtained using eq 3 for MA3 and MA4 and eq 5 for MA1.

due to the smaller micellar ensemble size, which is controlled by the shorter PI−$(PI)_2$ corona. This translates into a larger D_s, implying that reorganization/reorganization processes are more relevant in contrast with mass transport. Sample MA3 has a larger K^2/D_{eff} value than MA4. This might be due to MA3 having a longer PI stem block (70 kDa versus 33 kDa), which may favor an easier reorganization because of single chain release and micelle break up; however, the differences in the adsorption profiles between these two samples are very subtle.

Although a full analysis of SLS and DLS measurements will be published separately,[21] it is worth noting that the D_{eff} values obtained from the fits at 30 μg/mL are almost 1 order of magnitude ($< 5\times$) smaller than those determined by DLS. This difference can be understood by noting that D_{eff} captures the near-surface behavior, whereas light scattering measures the self-diffusion in free solution. Additionally, D_{eff} comes from fitting the entire adsorption profile measured from the injection of the polymer solution to pseudoequilibrium. The values for the reorganization parameter, K, are of the same order of magnitude, $\sim 10^{-5}$ cm/s, as those obtained from studies of adsorption of lipid vesicles,[23,24] suggesting commonality with the adsorption behavior of surfactant-based, bioinspired systems. Despite substantial differences in molecular complexity (e.g., size, topology), it is possible to affirm that the preferential adsorption of these macromolecular ensembles share the same underlying physical features: mass transport toward the solid/fluid interface and a variety of dynamic surface relaxation/reorganization processes. These include effects such as micelle breakup to supply single chains, interaction of the corona chains with the substrate and subsequent redistribution of the micellar ensemble to expose core blocks, and reflection of micelles that fail to reorganize and adsorb. The surface morphology is presumed to be a layer of surface hemimicelles and preferentially adsorbed single chains, as has been theoretically predicted by Ligoure[29] for block copolymer micelles adsorbed from selective solvents and experimentally observed by techniques such as atomic force microscopy.[13] AFM images, albeit of dried layers, seem to support this inference, as can be seen in the Supporting Information.

Further demonstration of the need to include both the diffusive and dynamic surface relaxation/reorganization contributions to properly describe the adsorption kinetics is obtained from experimental results at lower concentration. Figure 4 depicts the adsorption profile for MA3 at C_o = 3 μg/mL, with the inset scaled to highlight the early stages of the adsorption. A clear indication of the effect of reduced adsorbate concentration is that the time required to reach the pseudoequilibrium in Γ is now ~45 000 s, as compared with ~12 000 s observed at C_o = 30 μg/mL. It is also evident that a diffusion-controlled model (eq 4) provides a better description of the very early stages of adsorption at this concentration; however; the diffusion-limited fit yields a Γ_m = 1.25 mg/m^2, which differs substantially from the measured value, $\Gamma_{m,measured}$ = 0.97 mg/m^2. The kinetically controlled model (eq 5) yields a slightly lower Γ_m than what is measured at the pseudoplateau, but as shown in the inset in Figure 4, the agreement between the data and this limiting-case model at early times is rather poor. Consequently, a mixed-controlled model provides a much better description of the entire preferential adsorption process, closely following the layer evolution up to its pseudoequilibrium. Figure 5 shows the adsorption profiles for all the miktoarm samples at C_o = 3 μg/mL. The D_{eff} values obtained by fitting the results at 3 μg/mL are an order of magnitude larger than the ones obtained at 30 μg/mL, showing the increasing effect of surface reorganization with respect to mass transport. (See Table 2.) Here the parameter K^2/D_{eff} also provides evidence of the importance of dynamic relaxation/reorganization phenomena as the overall solution concentration decreases. Comparing the results at C_o = 30 and 3 μg/mL for samples MA3 and MA4, the decrease in K^2/D_{eff} in conjunction with the larger D_{eff} values ($\sim 10^{-7}$ cm^2/s) shows the enhanced role of the surface relaxation/reorganization processes on the adsorption kinetics. This is also reflected in the long times required (~45 000 s) to reach pseudoequilibrium at low concentration because the characteristic time scale of the dynamic relaxation/reorganization events are long and the flux of new ensembles to the surface is low. It is also found that the adsorption of the smallest copolymer, MA1 at C_o = 3 μg/mL, is best described by the limiting case where adsorption is dominated by dynamic relaxation/reoganization processes at the surface (eq 5) rather than a diffusion-limited model or the mixed-controlled model. Therefore, for small size micelles at a lower concentration, K^2/D_{eff} is smaller, suggesting that relaxation or reorganization of the micelles becomes a more prominent factor in the adsorption process. DLS experiments for sample MA3 at 3 μg/mL showed the coexistence of spherical micellar ensembles with smaller aggregates, unimers, or both in solution.[21] This observation helps to explain the much smaller K^2/D_{eff} value for MA3 with respect to MA4 as well as the prolonged time over which the

diffusion-controlled model provides a good fit during the initial stages of adsorption. (See Figure 4.) DLS experiments at 3 μg/mL for MA4 did not show any significant difference in the dynamic behavior of the micellar aggregates and thus explain the fact that there is only a minor change in the K^2/D_{eff} value for MA4 in comparison with the one determined at 30 μg/mL. It is interesting to note that at 30 μg/mL the adsorption profiles for MA3 and MA4 are quite similar, whereas at 3 μg/mL, they differ significantly.

The initial fast increase in Γ observed at both concentrations comes from the large availability of surface sites, where there is no competition or interaction between absorbing ensembles or macromolecules. In these initial stages, the near-surface concentration profile evolves, mainly controlled by the diffusion of material toward the solid/fluid interface but also because micelle adsorption is neither instantaneous nor assured. Whereas the near-surface concentration profile changes throughout the adsorption process, the dynamic relaxation/reorganization events occurring between the micelles and free chains in solution and of the adsorbed chains at the interface dominate the evolution of the interfacial layer. As the overall solution concentration decreases, the flux of polymer to the interface decreases; therefore, longer times are required to reach pseudoequilibrium. However, the same diffusion and relaxation/reorganization processes take place to generate the polymer layer on the surface.

Conclusions

The present work clarifies the important and controlling role of dynamic relaxation/reorganization events that occur throughout self-assembly (adsorption) of soft matter at the solid/fluid interface. In the micellar systems studied, the evolution of the interfacial layer toward pseudoequilibrium is the product of both the diffusion of macromolecular ensembles and the relaxation/reorganization events required to allow the PI corona chains to interact with the substrate and subsequently expose the PS core blocks to the substrate. This evolution is affected by the micelles and free chains in solution, the adsorbed chains at the already-populated surface, and the imperfect adsorption of the macromolecular ensembles, with the diffusion-limited regime described by Fick's second law ending quickly, even at ultralow concentrations. The mixed-controlled model successfully describes the kinetics of preferential adsorption from early stages to pseudoequilibrium and provides a quantitative basis for understanding the physical phenomena governing interfacial layer formation. A clear challenge remaining is to link ensemble structure, dynamics, and specific surface relaxation processes to the rate constant that represents these complex processes. Such closure would bring a fundamental understanding that connects macromolecular design, (supra) molecular assembly, and formation of polymer-modified interfaces by self-assembly.

Acknowledgment. Donors of the Petroleum Research Fund, administered by the American Chemical Society, are gratefully acknowledged for partial support of this work. A portion of this work was conducted at the Center for Nanophase Materials Sciences (enabled through user project 2008-297), which is sponsored at Oak Ridge National Laboratory by the Division of Scientific User Facilities, U.S. Department of Energy.

Supporting Information Available: Control adsorption experiments of the DB sample and a PI homopolymer sample are presented. The spreading coefficient S for both PS and PI in *n*-hexane on silicon is calculated. AFM images of the dry layer for sample MA3 adsorbed from *n*-hexane at 30 μg/mL is shown as a typical result. This material is available free of charge via the Internet at http://pubs.acs.org.

References and Notes

(1) Hadjichristidis, N.; Pispas, S.; Floudas, G. *Block Copolymers: Synthesis Strategies, Physical Properties, and Applications*; Wiley-Interscience: Hoboken, NJ, 2003; p 195.
(2) Hamley, I. W. *The Physics of Block Copolymers*; Oxford University Press: Oxford, U.K., 1998; p 131.
(3) Awan, M.; Dimonie, V.; Ou-Yang, D.; El-Aasset, M. *Langmuir* **1997**, *13*, 140.
(4) Zhulina, E.; Adam, M.; LaRue, I.; Sheiko, S.; Rubinstein, M. *Macromolecules* **2005**, *38*, 5330.
(5) Johner, A.; Joanny, J. *Macromolecules* **1990**, *23*, 5299.
(6) Gohy, J.-F. *Adv. Polym. Sci.* **2005**, *190*, 65.
(7) Sakai, K.; Smith, E.; Webber, G.; Schatz, C.; Wanless, E.; Bütün, V.; Armes, S.; Bigss, S. *J. Phys. Chem. B* **2006**, *110*, 14744.
(8) Toomey, R.; Mays, J.; Yang, J.; Tirrell, M. *Macromolecules* **2006**, *39*, 2262.
(9) Munch, M.; Gast, A. *Macromolecules* **1990**, *23*, 2313.
(10) Amiel, C.; Sikka, M.; Schneider, J.; Tsao, Y.-H.; Tirrell, M.; Mays, J. *Macromolecules* **1995**, *28*, 3125.
(11) Toomey, R.; Mays, J.; Holley, D.; Tirrell, M. *Macromolecules* **2005**, *38*, 5137.
(12) Zhan, Y.; Mattice, W. *Macromolecules* **1994**, *27*, 638.
(13) Hamley, I. W. *Block Copolymers in Solution: Fundamentals and Applications*; Wiley: Chichester, U.K., 2005; p 226.
(14) Dorgam, J.; Stamm, M.; Toprakcioglu, C.; Jérôme, R.; Fetters, L. *Macromolecules* **1993**, *26*, 5321.
(15) Motschmann, H.; Stamm, M.; Toprakcioglu, C. *Macromolecules* **1991**, *24*, 3681.
(16) Toomey, R.; Mays, J.; Tirrell, M. *Macromolecules* **2004**, *37*, 905.
(17) Alonzo, J.; Huang, Z.; Liu, M.; Mays, J.; Toomey, R.; Dadmun, M.; Kilbey, S. M., II. *Macromolecules* **2006**, *39*, 8434.
(18) Brandani, P.; Stroeve, P. *Macromolecules* **2003**, *36*, 9502.
(19) Erban, R.; Champman, J. *Phys. Rev. E* **2007**, *75*, 041116.
(20) Uhrig, D.; Mays, J. W. *J. Polym. Sci., Part A: Polym. Chem.* **2005**, *43*, 6179.
(21) Hinestrosa, J. P.; Alonzo, J.; Osa, M.; Mays, J.; Kilbey, S. M., II. manuscript in preparation.
(22) Parsonage, E.; Tirell, M.; Watanabe, H.; Nuzzo, R. *Macromolecules* **1991**, *24*, 1987.
(23) Hubbard, J.; Silin, V.; Plant, A. *Biophys. Chem.* **1998**, *75*, 163.
(24) Stroumpoulis, D.; Parra, A.; Tirrell, M. *AIChE J.* **2006**, *52*, 2931.
(25) Bijsterbosch, H.; Cohen Stuart, M.; Fleer, G. *Macromolecules* **1998**, *31*, 9281.
(26) LaRue, I.; Adam, M.; Zhulina, E.; Rubinstein, M.; Pisikalis, M.; Hadjichistidis, N.; Ivanov, D.; Gearba, R.; Anokhin, D.; Sheiko, S. *Macromolecules* **2008**, *41*, 6555.
(27) Sotiriou, K.; Nannou, A.; Velis, G.; Pispas, S. *Macromolecules* **2002**, *35*, 4106.
(28) Halperin, A.; Alexander, S. *Macromolecules* **1989**, *22*, 2403.
(29) Ligoure, C. *Macromolecules* **1991**, *24*, 2968.